

Recent Progress in Solving the Phase Problem in Surface and Interface Crystallography

Wataru Yashiro

Graduate School of Frontier Science, the University of Tokyo, 5-1-5 Kashiwanoha, Kashiwa-shi, Chiba 277-8561, Japan
Fax: 81-471-36-3997, e-mail: yashiro@mml.k.u-tokyo.ac.jp

Determining electron density in a material model-independently by X-ray diffraction has been a critical problem and actively studied since the middle of the 20th century. All the information that can be experimentally obtained by X-ray diffraction is only on intensity distribution, so that the information on the phase of scattering amplitude is lost, which prevents us from retrieving electron density model-independently. This is the so-called 'phase problem'. The phase problem in surface and interface crystallography has been one of interesting subjects in recent years. The present paper will focus on recent progress in solving the phase problem in surface and interface crystallography.

Key words: X-ray diffraction, surface, interface, crystallography, phase problem

1. INTRODUCTION

In the X-ray crystallography determining electron density in a material model-independently has been studied for a long time. Electron density can be determined by the Fourier transform of the complex scattering amplitude of the material. But all the information that can be experimentally obtained by X-ray diffraction is only on intensity distribution, so that the information on the phase of the scattering amplitude is lost. This makes it difficult to retrieve the electron density model-independently. Since the middle of the 20th century, many solutions to this 'phase problem' have been proposed, including direct methods [1-2], multiwavelength measurement [3], multibeam techniques [4], and X-ray holography [5,6].

The phase problem in surface and interface crystallography has been one of interesting subjects in recent years. Since the interaction of X-rays with a material is much smaller than that of electrons, structure analysis of crystal surface using X-ray diffraction is not possible without high intensity X-ray sources. Use of X-rays allows easy-to-interpret and high-precision analysis, which is generally difficult in the analysis of electron diffraction due to multiple scattering. Since the advent of the synchrotron radiation sources in the early 1980s, X-ray diffraction analysis has become a powerful tool for the structure analysis of crystal surface [7-11]. In the surface X-ray diffraction analysis, intensity distribution along crystal-truncation-rods (CTRs) [8] perpendicular to the crystal surface is measured, and compared with that calculated for several structure models which are physically possible. To determine three-dimensional atomic coordinates or, ultimately, electron density of crystal surface model-independently, the phase of the scattering amplitude along the CTRs has to be retrieved, which is the reason why conventional methods for solving the phase problem in X-ray crystallography cannot be applied to the surface X-ray diffraction analysis as it is. Various special methods have been developed since the middle of the 1980s, and more actively studied for the last decade. This paper will

focus on the recent progress in solving the phase problem in surface and interface crystallography. Several special and general methods are introduced, including the heavy atom method [12,13], the X-ray multibeam technique [14-21], and direct methods [22-36].

2. HEAVY ATOM METHOD

In the X-ray crystallography, the situation where there is one heavy atom per unit cell is desirable because it can help to solve the phase problem [37]. If the heavy atom is taken to be at the crystallographic origin, the phases of all structure factors are close to zero. As a result the Patterson (pair-correlation) function, which is calculated directly from the experimentally obtained intensity by the Fourier transform, is then very similar to a Fourier electron density map of the structure. This heavy atom method has been also applied to surface structure analysis [12,13]. Recently I.K. Robinson *et al.* applied the method to the structure analysis of quantum wires in Au/Si(557) [13]. They showed from X-ray diffraction data that the unit cell contains one Au atom and several Si atoms. For this structure the strongest peaks (apart from the origin) in the Patterson map correspond to Au-Si vectors; the Au is referred to as an "imaging" atom [37]. In Fig. 1 the Patterson map is given. This map is a superposition of the (x,z) and $(-x, -z)$ Si positions with respect to the Au at the origin. The Patterson map suggests specific atomic models, which can then be tested directly with the measured X-ray diffraction data. The model read off from the Patterson map is shown in Fig. 2. The step-edge Si atom identified as "B" in both Figs. 1 and 2 (b) has very little density in the map and is a clear candidate for omission; for this to happen, the edge could reconstruct by forming five-membered rings as shown by the dashed bonding line. The additional peak marked "C" is near the correct position for an "adatom" that could accommodate three otherwise dangling bonds on the terrace in every other unit cell (along y), thus appearing to have an occupation

of 50% in the 1×1 cell. Models were built with combinations of these features and tested against the data using the ROD program [38] with a total of 47 free positional parameters, variable occupancy for the Au, and Debye-Waller factors (DWF) for the atoms near the step edge. Both the missing edge atom B and the adatom C were supported upon refinement of all the atomic positions in the outermost two double layers of the structure. The best agreement without the adatom was $\chi^2 = 7.5$ which dropped to $\chi^2 = 7.1$ with the adatom included. The refined coordinates of the final model are shown in Fig. 2 (c).

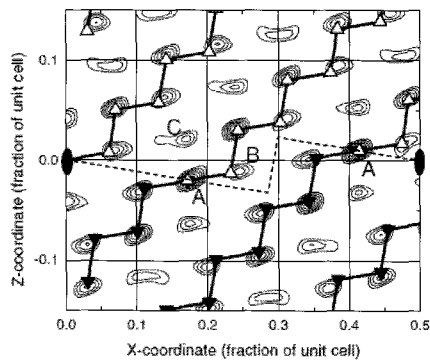


Fig.1 Positive contours of the $y = 0$ section of the Patterson function obtained directly by Fourier transformation of the CTR intensities observed for Au/Si(557). The map has twofold rotational symmetry about the origin ($x = 0, z = 0$) (peak suppressed), and about the center ($x = 1/2, z = 0$), as shown by diad symbols. Because the unit cell is centered, the $y = 1/2$ section can be obtained by a shift of $1/2$ in x . The interpretation drawn assumes Au at the origin and Si atoms at all the other peaks. This identifies the termination (dashed line). (Reprinted figure with permission from [13]. Copyright 2002 by the American Physical Society).

3. MULTIBEAM TECHNIQUES

In X-ray multiple diffraction where more than one Bragg reflections are excited simultaneously, the intensities of the diffracted beams depend on the relative phases of the structure factors involved [4]. This fact has been also applied to retrieve the information on the phase of the scattering amplitude of surface structure [14-21]. Here the author introduces two examples of multibeam technique recently proposed.

3.1 Two beam diffraction interference (TBDI) method

The two beam diffraction interference (TBDI) method was proposed by Yacoby *et al* [14,15,17]. If a sample with a two dimensional periodicity is on a substrate or under an overlayer consisting of heavier atom, the total reflection occurs at small incidence angles to the interface. In the TBDI method intensities along a CTR are measured under this condition, where the incident and reflected beam are diffracted by the sample and interfere with each other. This provides the phase derivative along the CTR. This method was tested to a GaAs/AlAs/GaAs (Fig. 3 (a)), the result of which is shown in Fig. 3 (b) with a result of COBRA (see the Section 4.1) [17].

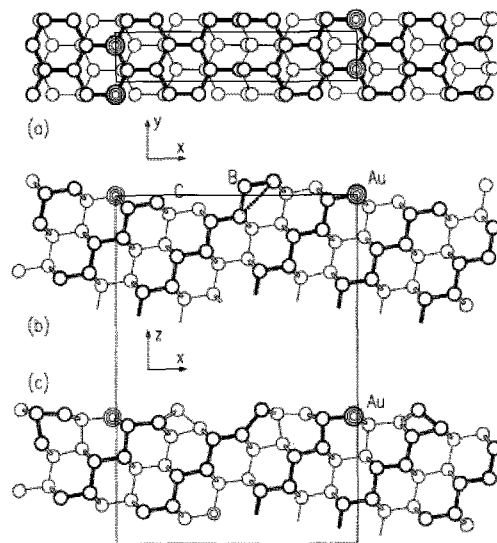


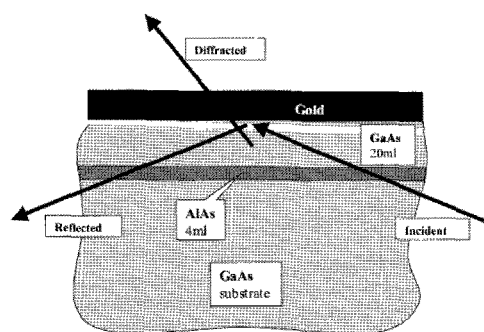
Fig. 2 Structural models of the Au/Si(557) surface. The Au atom is drawn as a triple circle. The boxes show half a unit cell in both x and z and a full cell in y , offset for clarity. (a) Top view. (b) Side view of the model read directly from the Patterson map indicating the locations of peaks "B" and "C." (c) Final model after refinement of atomic positions. Atoms and bonds closer to the viewer are drawn with heavier lines to create perspective. (Reprinted figure with permission from [13]. Copyright 2002 by the American Physical Society).

3.2 Method using a Bragg reflection

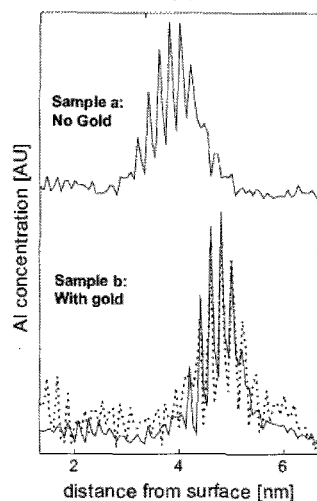
A method using a Bragg reflection from the substrate crystal was proposed by the author. Although this method can be applied to a special case where the substrate is nearly perfect crystal, it allows a high precision measurement, which has led to a new knowledge about strain field under the SiO_2/Si interface which has never been revealed by the conventional X-ray diffraction measurement. Here the author introduces the application of this method to characterize the strain field under the $\text{SiO}_2/\text{Si}(001)$ interface.

Our method is an application of a phenomenon, modulation of the intensity of the CTR scattering under an excitation of a Bragg reflection [18-21,39], which is an interaction between a CTR scattering and a Bragg reflection. By using this technique the author revealed that there is a small strain field extending over mesoscopic-range depth (up to several hundred of nm) under the $\text{SiO}_2/\text{Si}(001)$ interface and having a static fluctuation in the lateral direction [21].

An example of the phenomenon in the case of the Si(001) wafer is shown in Fig. 4, where intensity of the 50 rod CTR scattering is modulated by the excitation of the 004 Bragg reflection. We showed that the modulation profile can be characterized by only two parameters: the phase shift, which represents the dip or peak position of the modulation profile, and the visibility. The phase shift is directly related to the phases of the scattering amplitudes of CTR scatterings, and can be simply interpreted into the sum of displacements of atomic planes under the interface, which is due to the strain field extending over mesoscopic-range depth, while the visibility gives information on static



(a)



(b)

Fig. 3 (a) The schematic diagram of the sample and scattering geometry. (b) The experimentally obtained electron density difference between an ideal GaAs semi-infinite crystal and two GaAs/AlAs samples. Dotted line: analysis with the phase derivative using the TBDI method; solid lines: analysis with the COBRA (see the Section 4.1). (Reprinted figure with permission from [17]. Copyright 2000 by the Institute of Physics (IOP) Publishing Ltd.)

fluctuation of the total displacement in the lateral direction [21]. The solid line in Fig. 4 is the best-fit curve calculated, where the phase shift and visibility are fixed at $-2\pi \times (0.117 \pm 0.001)$ and 0.521 ± 0.002 . Both the experimentally obtained values were different from those of an ideal perfect crystal (0 and 0.711, respectively), which is shown by the dotted line in the figure.

Figure 5 shows an illustration of the strain field under the $\text{SiO}_2/\text{Si}(001)$ interface which can explain the experimentally obtained modulation profile. The phase shift corresponds to the sum of displacements of atomic planes under the interface projected onto the direction perpendicular to the 004 plane (-0.16 \AA in the figure). On the other hand the visibility indicates that the total displacement has a static fluctuation of at least $\pm 0.13 \text{ \AA}$ in the direction parallel to the interface. The features revealed by this technique are expected to provide a new window to understand the oxidation mechanism of Si surface.

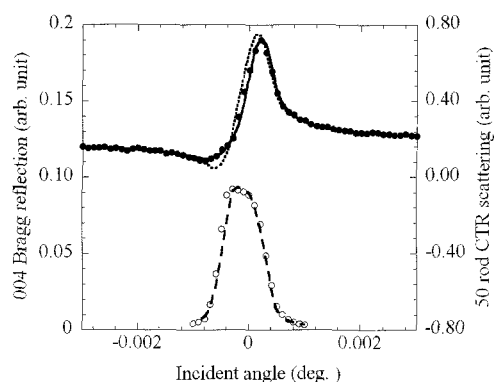


Fig. 4 Intensity of the CTR scattering is modulated by the excitation of a Bragg reflection [18-21,39]. An example is demonstrated in the case of a $\text{Si}(001)$ wafer covered with a thermal oxide layer. The solid and open circles represent the experimentally obtained intensities corresponding to the 50 rod CTR scattering and 004 Bragg reflection, whose scales (in arbitrary units) are on the right and left axes, respectively. The horizontal axis is the deviation in the incident angle from the 004 Bragg angle. The dotted line is the intensity calculated for an ideal perfect crystal. The solid and broken lines are the best-fit curves to the experimentally obtained data [21].

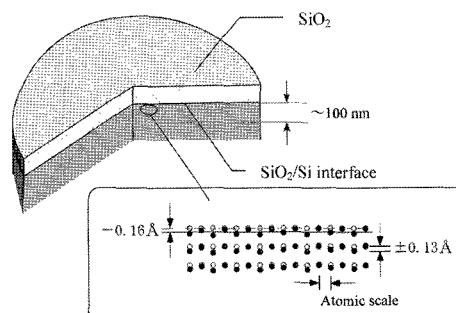


Fig. 5 Illustration of the strain field under the $\text{SiO}_2/\text{Si}(001)$ interface which can explain the experimentally obtained modulation profile in Fig. 4. The open circles represent to the sites of atoms or unit cells in bulk crystal, and the solid circles represent the position of them in the strained layer near the interface.

4. DIRECT METHODS

The aim of the direct method in the surface structure analysis is to guess the phase of the scattering amplitude along the CTRs directly from the intensities on the rods. Recently several methods were proposed: the coherent Bragg rod analysis (COBRA) [17,22,23], holographic imaging using intensities along integer order rods [24,25], the maximum entropy method (MEM) [26], and the methods based on the Sayre's equation [27-29], and the Gerchberg-Saxton and Fienup algorithms [30-36].

4.1 Coherent Bragg rod analysis method (COBRA)

In a general sense the total scattering intensity can be considered as coherently composed of two contributions: the scattering of a known reference electron density and that of an unknown electron density such that the combination of the two yields the scattering of the

electron density of the real system. The reference part can be, for example, the known substrate and a simple model of the film. In this case the unknown electron density will be large within the film and the region of the substrate deformed by the film. At any two adjacent points along a Bragg rod differing by $\Delta\vec{k}$

$$S(\vec{k} - \frac{\Delta\vec{k}}{2}) + U(\vec{k} - \frac{\Delta\vec{k}}{2}) = T(\vec{k} - \frac{\Delta\vec{k}}{2}) \quad (1)$$

$$S(\vec{k} + \frac{\Delta\vec{k}}{2}) + U(\vec{k} + \frac{\Delta\vec{k}}{2}) = T(\vec{k} + \frac{\Delta\vec{k}}{2}) \quad (2)$$

where, S , U , and T are the complex scattering amplitudes due to the reference, unknown, and total electron densities, respectively. We now make use of the fact that the complex scattering amplitudes vary continuously along the Bragg rods and make the approximation that at two adjacent points along a Bragg rod:

$$U(\vec{k} - \frac{\Delta\vec{k}}{2}) \approx U(\vec{k} + \frac{\Delta\vec{k}}{2}) = U_a(\vec{k}) \quad (3)$$

This approximation is valid if $U(\vec{k})$ varies slowly relative to $S(\vec{k})$. Taking the absolute value of Eqs. (1) and (2) in this approximation yields

$$\left| S(\vec{k} - \frac{\Delta\vec{k}}{2}) + U_a(\vec{k}) \right| = \left| T(\vec{k} - \frac{\Delta\vec{k}}{2}) \right| \quad (4)$$

$$\left| S(\vec{k} + \frac{\Delta\vec{k}}{2}) + U_a(\vec{k}) \right| = \left| T(\vec{k} + \frac{\Delta\vec{k}}{2}) \right| \quad (5)$$

In Eqs. (4) and (5) the absolute values squared of the total scattering amplitudes are proportional to the experimentally determined intensity. This yields two real equations that can be solved for one complex unknown. In general this pair of equations has two solutions and it is necessary to choose the correct one. The correct solutions are obtained by looking at two pairs of equations at two consecutive pairs of points. This is shown in Fig. 6. The figure on the left represents the equations at $\vec{k} - \Delta\vec{k}/2$ and $\vec{k} + \Delta\vec{k}/2$. The corresponding complex numbers are marked with indices 1 and 2, respectively. The figure on the right represents the equations at $\vec{k} + \Delta\vec{k}/2$ and $\vec{k} + 3\Delta\vec{k}/2$ and the corresponding indices are 2 and 3, respectively. Each pair of equations has two solutions U_a and U_b shown as solid and dashed lines, respectively. Under the assumption that U varies slowly along the Bragg rods the correct pair of solutions is the one that changes the least when going from one point to the next; namely, (in Fig. 6) U_{1a} and U_{2a} . This procedure then provides the unknown complex scattering amplitudes along each Bragg rod. The electron density can be obtained by the Fourier transform of the complex scattering amplitudes into real space.

The usefulness of the COBRA was demonstrated by mapping the structure of the interfacial region of a Gd_2O_3 film grown epitaxially on a (100) GaAs substrate [22,23]. Two examples of the electron-density maps

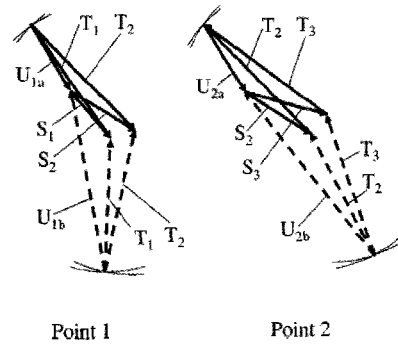


Fig. 6 Graphic representation of Eqs. (1) and (2) in the complex plane. The equations are shown for two pairs of adjacent points. S_1 , S_2 and S_3 are the known complex scattering amplitudes at $\vec{k} - \Delta\vec{k}/2$, $\vec{k} + \Delta\vec{k}/2$, and $\vec{k} + 3\Delta\vec{k}/2$, respectively. The total scattering amplitudes T are known only in absolute value so they are represented by arrows and arcs. U_{1a} and U_{2a} , U_{1b} and U_{2b} are two pairs of solutions. The correct solutions are those that vary the least when going from point 1 to point 2. Namely, in this case U_{1a} and U_{2a} . (Reprinted figure with permission from [22]. Copyright 2002 by the American Physical Society).

obtained by COBRA are shown in Fig.7. Each map consists of 3×3 GaAs 2D unit cells. Figure 7 (a) is the eighth layer below the interface on the GaAs side and Fig. 7 (b) is the ninth layer above the interface on the Gd_2O_3 side. The first map clearly shows the Ga or As atomic positions. The second shows the ridges and valleys expected from the folded structure (Because the periodicity of the Gd_2O_3 structure is a multiple of that of GaAs, the scattering amplitude along the GaAs-defined Bragg rods is the Fourier transform of the electron density folded into a GaAs-defined 2D unit cell). From such results they found that the Gd atoms in the first few Gd_2O_3 layers are locked in the substrate GaAs positions and that the stacking arrangement of the epitaxial film conforms to that of the substrate rather than that of bulk Gd_2O_3 .

4.2. Maximum entropy method (MEM)

Maximum-Entropy Method (MEM) originates with the information theory developed by Shannon, and is based on the principle of maximum entropy first expounded by E.T. Jaynes in 1957 [40]. M.D. Collins applied this method to the macromolecular X-ray crystallography. Recently D.K. Saldin *et al.* adapted the MEM to the surface X-ray crystallography, and successfully guessed 3D surface electron densities [26]. In the MEM the most probable distribution that is consistent with the experimental data is searched, which is attained by the Bayesian theorem of conditional probabilities. The detailed algorithm of the MEM is reported in the literature [26]. In the use of the MEM one has to be careful for the final result not to overfit the data, which often lead to unphysical results. This method was successfully applied to the structure analyses of $\text{K}/\text{Ag}(001)$, $\text{O}/\text{Cu}(104)$, and $\text{GaAs}(2 \times 2)$ [26].

4.3 Method based on the Sayre's equation

A way to extend the direct method based on the Sayre's equation [42] that has been used in the X-ray

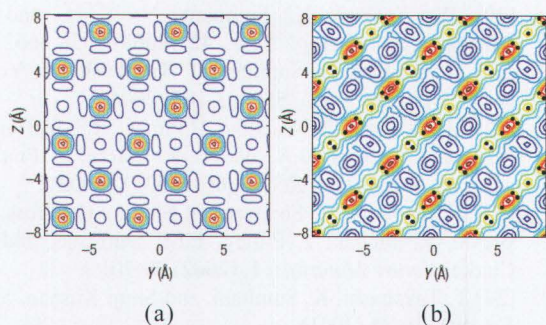


Fig. 7 COBRA electron-density maps of Gd_2O_3 -GaAs (100) epitaxial structure. Low density, cold colors; high density, warm colors. (a) Eighth Ga/As monolayer below the nominal interface; (b) Ninth Gd_2O_3 layer above the interface. The black dots are the folded bulk in-plane Gd positions. Y and Z denote the position within a particular plane parallel to the interface. (Reprinted by permission from Macmillan Publishers Ltd: Nature Materials [23], copyright 2002).

crystallography to the surface structure analysis was proposed by L.D. Marks [27,28]. In his approach a set of phases is determined with the lowest figures of merit, which is most consistent with the measured experimental data, using statistical (probabilistic) relationships between the modulus and the phase of the scattering amplitudes. In the phase recovery process positivity (the electron density must be real and positive) and 'support constraint' (the surface charge density normal to the surface must be zero except in small region near the surface) are imposed. Here experimental data has to be sampled along CTRs at a frequency greater than twice that required by the size of the support region. By this approach scattering potential maps and candidate structures can be generated from the experimental data without the need for a structure guess (an example is shown in Fig. 8 [29]).

4.4 Method based on the Gerchberg-Saxton and Fienup algorithms

The algorithm [30-36] originates with the iterative phase recovery strategy of Gerchberg and Saxton [43], Fienup [44,45], which is also applied to the X-ray diffraction microscopy [46] and the coherent X-ray diffraction imaging for nanocrystals [47]. The iterative phase recovery algorithm is depicted in Fig. 9. Initially, a random set of phases $\{\phi\}$ is assigned to the experimentally observed structure factor amplitudes $\{|F_{\text{obs}}|\}$. After subtracting the calculable bulk contribution $\{B\}$, a Fourier transform renders an estimate in real space of the electron density $\{t\}$ in the near-surface region.

Next invoke a physically reasonable constraint (spatial support) is imposed: the surface electron density must lie only within a few angstroms of the surface, giving an improved estimate $\{u\}$ of the surface electron density. Then, an inverse Fourier transform of $\{u\}$, namely the set $\{S_{\text{calc}}\}$ of surface structure factors is added to the calculated bulk contribution $\{B\}$. The arguments of the sums represent improved estimates of the phases $\{\phi\}$. A constraint in reciprocal space is finally imposed by assigning these phases to the experimentally

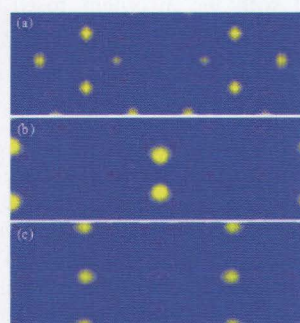


Fig. 8 [(a)-(c)] Electron density maps for the centered (6×2) unit cell from SXRD direct methods at $z = 3.6 \text{ \AA}$, $z = 2.8 \text{ \AA}$, and $z = 2.0 \text{ \AA}$ above the first bulklike TiO_2 layer, respectively. Regions of high electron density (possible atomic sites) are yellow (light). (Reprinted figure with permission from [29]. Copyright 2007 by the American Physical Society).

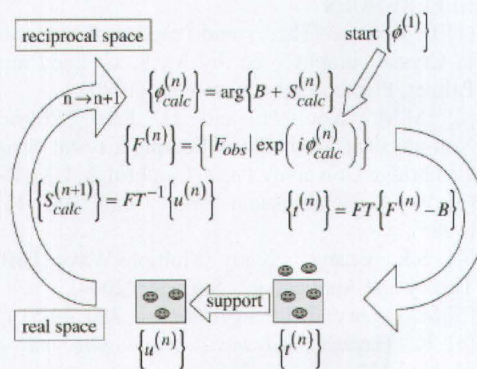


Fig. 9 Schematic flowchart of the iterative algorithm. (Reprinted figure with permission from [32]. Copyright 2005 by the American Physical Society).

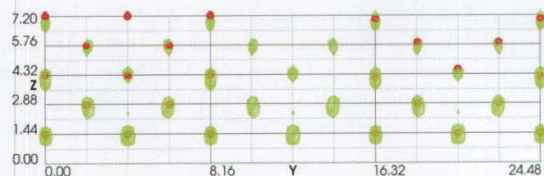


Fig. 10 $[1 \bar{1} 0]$ projection of the recovered electron density. The (2×1) surface unit cell is repeated three times. The black balls on the left are shown at bulk-terminated locations, while those on the right are positioned according to conventional χ^2 refinement. (Reprinted figure with permission from [32]. Copyright 2005 by the American Physical Society).

observed structure factor amplitudes $\{|F_{\text{obs}}|\}$, and the cycle is repeated. Thus, by alternately imposing these constraints in real and reciprocal space, $\{u\}$ converges with a solution that is confined to the near-surface region and agrees with the experimental scattering data. It is not assumed that scattering arises from atoms, but rather recover the continuous charge density. This algorithm successfully provided initial guess of structure of the well-known Au(110)- (2×1) [32,33] (see Fig. 10), Sb/Au(110)- $c(2 \times 2)$ [33,34], and Sb/Au(110)- $(\sqrt{3} \times \sqrt{3})$ R54.7° [33,35] surfaces. This approach was also

combined with the algorithm based on the Sayre's equation (the tangent formula iteration scheme) briefly described above [36].

5. SUMMARY

We have focused on recent progress in solving the phase problem in surface and interface crystallography. Various phase recovery methods have been proposed. Use of special methods, such as the heavy atom method and multibeam techniques, is limited to special samples, but, in some cases, much information on the surface structure may be inherently contained in the experimental data, which allows us to analyze complicated structures with high precision. General methods based on the Sayre's equation, and the Gerchberg-Saxton and Fienup algorithms are powerful tools, and, by combined with rapid measurements [48,49], they will make it possible to realize quick structure analysis of crystal surface.

REFERENCES

- [1] D. Rogers, "Theory and Practice of Direct Methods in Crystallography", ed. by M. F. C. Ladd and R. A. Palmer, Plenum Press, New York (1980).
- [2] M.M. Woolfson and H. Fan, "Physical and Non-physical Methods of Solving Crystal Structures", Cambridge University Press, Cambridge, UK (1995).
- [3] W. A. Hendrickson, *Phys. Today*, **48**, (11) 42-48 (1995).
- [4] S.L. Chang, "X-ray Multiple-Wave Diffraction: Theory and Application", Springer (2004).
- [5] M. Tegze and G. Faigel, *Nature*, **380**, 49-51 (1996).
- [6] K. Hayashi, *Advances in imaging and electron physics*, **140**, 119-185 (2006).
- [7] P. Eisenberger and W. C. Marra, *Phys. Rev. Lett.*, **46**, 1081 (1981).
- [8] I. K. Robinson, *Phys. Rev. B*, **33**, 3830-3836 (1986).
- [9] T. Takahashi, S. Nakatani, N. Okamoto, T. Ishikawa, and S. Kikuta, *Jpn. J. Appl. Phys.*, **27**, L753-755 (1988).
- [10] I. K. Robinson, *Handbook on Synchrotron Radiation*, ed. by G. Brown and D. E. Moncton (Elsevier Science Publishers B.V., 1991) Vol. 3, Chap. 7.
- [11] R. Feidenhans'l, *Surf. Sci. Rep.*, **10**, 105-188 (1989).
- [12] T. Takahashi, S. Nakatani, T. Ishikawa, and S. Kikuta, *Surf. Sci.*, **191**, L825-834 (1987).
- [13] I.K. Robinson, P.A. Bennett, and F.J. Himpsel, *Phys. Rev. Lett.*, **88**, (2002) 096104.
- [14] Y. Yacoby, *Solid State Commun.*, **91**, (1994) 529-533.
- [15] H. Baltés, Y. Yacoby, R. Pindak, R. Clarke, L. Pfeiffer and L. Berman, *Phys. Rev. Lett.*, **79**, 1285-1288 (1997).
- [16] S. L. Chang, Y. S. Huang, C. H. Chao, M. T. Tang and Y. P. Stetsko, *Phys. Rev. Lett.*, **80**, (1998) 301-304.
- [17] Y. Yacoby, R. Pindak, R. MacHarrie, L. Pfeiffer, L. Berman, and R. Clarke, *J. Phys.: Condens. Matter*, **12**, 3929-3938 (2000).
- [18] V. M. Kaganer, M. Albrecht, A. Hirnet, M. Gierer, W. Moritz, B. Jenichen, and K. H. Ploog, *Phys. Rev. B*, **61**, R16355-R16358 (2000).
- [19] T. Takahashi, W. Yashiro, M. Takahashi, S. Kusano, X.W. Zhang and M. Ando, *Phys. Rev. B*, **62**, 3630-3638 (2000).
- [20] W. Yashiro, K. Sumitani, Y. Yoda, and T. Takahashi, *Jpn. J. Appl. Phys.*, **42**, (2003) 6658-6662.
- [21] W. Yashiro, K. Sumitani, T. Takahashi, Y. Yoda, and K. Miki, *Surf. Sci.*, **550**, 93-105 (2004).
- [22] M. Sowwan, Y. Yacoby, J. Pitney, R. MacHarrie, M. Hong, J. Cross, D.A. Walko, R. Clarke, R. Pindak, and E.A. Stern, *Phys. Rev. B*, **66**, 205311 (2002).
- [23] Y. Yacoby, M. Sowwan, E. Stern, J.O. Cross, D. Brewster, R. Pindak, J. Pitney, E.M. Dufresne, and R. Clarke, *Nature Materials*, **1**, (2002) 99-101.
- [24] T. Takahashi, K. Sumitani, and Shuji Kusano, *Surf. Sci.* **493**, 36-41 (2001).
- [25] K. Sumitani, T. Takahashi, S. Natatani, A. Nojima, O. Sakata, Y. Yoda, S. Koh, T. Irisawa, and Y. Shiraki, *Jpn. J. Appl. Phys.* **42**, L189-191 (2003).
- [26] D.K. Saldin, R. Harder, H. Vogler, W. Moritz, I.K. Robinson, *Comp. Phys. Comm.*, **137** 12-24 (2001).
- [27] L.D. Marks, E. Bengu, C. Collazo-Davila, D. Grozea, E. Landree, C. Leslie, and W. Sinkler, *Surf. Rev. Lett.* **5**, 1087-1106 (1998).
- [28] L.D. Marks, *Phys. Rev. B*, **60**, 2771-2780 (1999).
- [29] C. H. Lanier, A. van de Walle, N. Erdman, E. Landree, O. Warschkow, A. Kazimirov, K. R. Poepelmeier, J. Zegenhagen, M. Asta, and L. D. Marks, *Phys. Rev. B*, **76**, 045421 (2007).
- [30] D.K. Saldin, R.J. Harder, V.L. Shneerson, and W. Moritz, *J. Phys.: Condens. Matter*, **13**, 10689-10707 (2001).
- [31] D.K. Saldin, R.J. Harder, V.L. Shneerson, and W. Moritz, *J. Phys. Condens. Matter*, **14**, 4087-4100 (2002).
- [32] P.F. Lyman, V.L. Shneerson, R. Fung, R.J. Harder, E.D. Lu, S.S. Parihar, and D.K. Saldin, *Phys. Rev. B*, **71**, 081402(R) (2005).
- [33] R. Fung, dissertation for the degree of PhD in physics at the university of Wisconsin-Milwaukee (2005).
- [34] P.F. Lyman, V.L. Shneerson, R. Fung, S.S. Parihar, H.T. Johnson-Steigelman, E.D. Lu, and D.K. Saldin, *Surf. Sci.*, **600**, 424-435 (2006).
- [35] R. Fung, V.L. Shneerson, P.F. Lyman, S.S. Parihar, H.T. Johnson-Steigelman, and D.K. Saldin, *Acta Cryst.* **A63**, 239-250 (2007).
- [36] D.K. Saldin, V.L. Shneerson, and R. Fung, *Physica B*, **336**, 16-26 (2003).
- [37] H. B. Dyer, *Acta Cryst.*, **4**, 42-50 (1951).
- [38] E. Vlieg, *J. Appl. Cryst.*, **33**, 401-405 (2000).
- [39] T. Takahashi and S. Nakatani, *Surf. Sci.* **326**, 347-360 (1995).
- [40] E.T. Jaynes, *Phys. Rev.*, **106**, 620-630 (1957).
- [41] M.D. Collins, *Nature*, **298**, 49-51 (1982).
- [42] D. Sayre, *Acta Cryst.*, **5**, 60-65 (1952).
- [43] R.W. Gerchberg and W.O. Saxton, *Optik*, **35**, 237 (1972).
- [44] J.R. Fienup, *Opt. Lett.*, **3**, 27-29 (1978).
- [45] J.R. Fienup, *Appl. Opt.*, **21**, 2758-2769 (1982).
- [46] J. Miao, P. Charalambous, J. Kirz, and D. Sayre, *Nature*, **400**, 342-344 (1999).
- [47] M.A. Pfeifer, G.J. Williams, I.A. Vartanyants, R. Harder, and I.K. Robinson, *Nature*, **442**, 63-66 (2006).
- [48] O. Sakata, W. Yashiro, D.R. Bowler, A. Kitano, K. Sakamoto, and K. Miki, *Phys. Rev. B*, **72**, 121407 (2005).
- [49] H. Tajiri, O. Sakata, and T. Takahashi, *Appl. Surf. Sci.*, **234**, 403-408 (2004).